Phase separation and size effects in $Pr_{0.70}Ba_{0.30}MnO_{3+\delta}$ perovskite manganites

2007 J. Phys.: Condens. Matter 19 266214

(http://iopscience.iop.org/0953-8984/19/26/266214)

IOP PUBLISHING JOURNAL OF PHYSICS: CONDENSED MATTER

J. Phys.: Condens. Matter **19** (2007) 266214 (18pp) doi:10.1088/0953-8984/19/26/266214

Phase separation and size effects in $Pr_{0.70}Ba_{0.30}MnO_{3+\delta}$ perovskite manganites

S V Trukhanov[1], A V Trukhanov[2], C E Botez[3], A H Adair[3], H Szymczak[4] and R Szymczak[4]

[1] Joint Institute of Solids and Semiconductor Physics of NAS of Belarus, P Brovka street 19, 220072 Minsk, Belarus
[2] Chemistry Department, Vitebsk State University, Moscow Avenue 33, 210036 Vitebsk, Belarus
[3] Physics Department, The University of Texas at El Paso, El Paso, TX 79968, USA
[4] Institute of Physics, PAS, Lotnikov street 32/46, 02-668 Warsaw, Poland

E-mail: truhanov@ifttp.bas-net.by (S V Trukhanov)

Received 5 March 2007, in final form 24 May 2007
Published 14 June 2007
Online at stacks.iop.org/JPhysCM/19/266214

Abstract

The crystal structure and magnetotransport properties of the A-site ionic ordered state in $Pr_{0.70}Ba_{0.30}MnO_{3+\delta}$ ($\delta = 0$, 0.025) have been investigated. It is shown that such a state can be formed in complex manganites with cation ratios $Pr^{3+}/Ba^{2+} \gg 1$ by using a 'two-step' reduction–reoxidization method. The parent A-site ionic disordered $Pr_{0.70}Ba_{0.30}MnO_{3+\delta}$ ($\delta = 0$) compound is an orthorhombic (SG = $Imma$, $Z = 4$) ferromagnet with Curie temperature $T_C \approx 173$ K and ground-state spontaneous magnetic moment $\sigma_S \sim 3.70$ μ_B/f.u. It exhibits two metal–insulator transitions, at $T_I \sim 128$ K and $T_{II} \sim 173$ K, as well as two peaks of magnetoresistance ~74% and ~79% in a field of 50 kOe. The parent A-site ionic disordered $Pr_{0.70}Ba_{0.30}MnO_{3+\delta}$ ($\delta = 0$) sample used in our studies has an average grain size $\langle D \rangle \approx 10.213$ μm. Successive annealing of this sample in vacuum $P[O_2] \approx 10^{-4}$ Pa and then in air at $T = 800\,^{\circ}$C leads to the destruction of its initial grain structure and to its chemical separation into two phases: (i) oxygen stoichiometric A-site ordered $PrBaMn_2O_6$ with a tetragonal (SG = $P4/mmm$, $Z = 2$) perovskite-like unit cell and Curie temperature $T_C \approx 313$ K and (ii) oxygen superstoichiometric A-site disordered $Pr_{0.90}Ba_{0.10}MnO_{3.05}$ with an orthorhombic (SG = $Pnma$, $Z = 4$) perovskite-like unit cell and Curie temperature $T_C \approx 133$ K. This processed sample has a spontaneous magnetic moment $\sigma_S \sim 2.82$ μ_B/f.u. in its ground state, and $\sigma_S \sim 0.59$ μ_B/f.u. at $T \sim 300$ K. It also exhibits a magnetoresistance of ~14% at ~313 K in a field of 50 kOe. This processed sample has a reduced average grain size $\langle D \rangle \approx 491$ nm. The two magnetic phases, $Pr_{0.90}Ba_{0.10}MnO_{3.05}$ and $PrBaMn_2O_6$, are exchange-coupled. For $Pr_{0.90}Ba_{0.10}MnO_{3.05}$ the temperature hysteresis is ~22 K in a field of 10 Oe and ~5 K in a field of 1 kOe. The observed magnetic properties are interpreted in terms of chemical phase separation, grain size, and A-site ionic ordering effects.

1. Introduction

Complex manganese oxides $Ln_{1-x}D_xMnO_3$ (Ln—La–Dy trivalent lanthanide, D—Ca, Sr, Ba divalent alkaline earth metal) with perovskite crystal structure have been investigated extensively [1–5] due to their remarkable electrical and magnetic properties, which include the so-called colossal magnetoresistive effect [6–8]. While many factors determine the properties of manganites, the most important ones are their electronic structure, which is related to the ion type and stoichiometry, and their crystal structure, where the average ⟨Mn–O⟩ bond length and the average ⟨Mn–O–Mn⟩ bond angle play key roles.

Basically, undoped $LnMnO_3$ manganites are orbitally ordered A-type antiferromagnetic insulators, where the paramagnet–antiferromagnet transition temperature shifts toward lower values with the decrease in the lanthanide ion radius. Consequently, samples based on La^{3+}, Pr^{3+} and Nd^{3+} have Neel temperatures $T_N \sim 141$ K [9], ∼99 K [10, 11] and ∼88 K [11, 12], respectively. Samples based on Sm^{3+}, Eu^{3+}, Gd^{3+}, Tb^{3+} and Dy^{3+} are spin glasses. For these materials the decrease in the lanthanide ion radius leads to a decrease in the average ⟨Mn–O–Mn⟩ bond angle from 180° [13], and to the reduction in both the e_g-electron bandwidth, $W = \cos(1/2[\pi - \langle \text{Mn–O–Mn} \rangle])/\langle \text{Mn–O} \rangle^{3.5}$ [14], and the e_g-electron transfer integral, $b_{ij} = b_{ij}^0 \cos(\theta_{ij}/2)$ [15]. Here, $b_{ij}^0 \sim \langle$Mn–O–Mn$\rangle$ and θ_{ij} is the angle between neighbouring S_i and S_j spins.

For complex doped $Ln_{1-x}D_xMnO_3$ manganites, increasing the dopant concentration x induces a transformation from an antiferromagnetic insulator to a ferromagnetic metal. For $0.2 < x < 0.5$ these materials (Ln—La^{3+}, Pr^{3+}, Nd^{3+} and D—Sr^{2+}, Ba^{2+}) are in a ferromagnetic metallic state below the Curie temperature T_C due to the dominant role of the ferromagnetic double exchange [16]. The maximum values of T_C are reached for the optimal doping $x \sim 0.3$ [1, 17]. Moreover, for a given hole concentration, the magnetotransport properties of the doped manganites are determined not only by the average A-site ionic radius, $\langle r_A \rangle = (1-x)r_{Ln} + xr_D$ [18], but also by the size mismatch at the A site, represented by the variance $\sigma^2 = \sum_i x_i r_i^2 - \langle r_A \rangle^2$ (where i is the A-site cation type) [19]. Indeed, it was found that the increase in σ^2 (at constant $\langle r_A \rangle$) induces local distortions in the crystal structure, which, in turn, reduces the average ⟨Mn–O–Mn⟩ bond angle to values below 180° [20] and leads to significantly lower Curie temperatures [21].

Several theoretical models have been developed in an attempt to explain the physical properties of complex manganites, including double exchange interactions [16, 17], superexchange interactions [22, 23], or phase separations with competitive exchange interactions having opposite signs [24, 25]. Yet, a universal theoretical model should also take into account the influence of higher-order effects, such as the presence of various defects and inhomogeneities. Among these, cation ordering in the perovskite structure is known to noticeably alter the magnetotransport properties of manganites even when $\langle r_A \rangle$ and σ^2 have fixed values.

For example, $La_{0.50}Ba_{0.50}MnO_3$ ($\langle r_A \rangle = 1.3430$ Å, $\sigma^2 = 0.0161$ Å^2) is a metallic ferromagnet below ∼270 K in its A-site disordered form, but has $T_C \sim 335$ K in its A-site ordered form [26]. In the A-site ordered form, alternating planes of LaO and BaO separate MnO_2 sheets in such a way that each $Mn^{3+/4+}$ ion has four La^{3+} neighbours in one direction and four Ba^{2+} neighbours in the opposite direction, which makes all the Mn^{3+}/Mn^{4+} ions equivalent. In the A-site disordered form, however, La^{3+} and Ba^{2+} cations are randomly distributed and Mn^{3+}/Mn^{4+} are surrounded by different combinations of divalent and trivalent cations. The different chemical environments result in different chemical pressures on the Mn^{3+}/Mn^{4+} ions, which is a source of disorder in the Mn^{3+}/Mn^{4+} electronic levels [27–29]. For the A-site ordered $LaBaMn_2O_6$ compound, the ferromagnetic phase coexists with the CE-

type antiferromagnetic phase. This confirms the fact that the electron phase separation is not only the result of random filling of the A-sublattice, but is also determined by the competition of superexchange interactions with charge ordering. The latter, in turn, is strongly affected by minute changes in the local crystal structure at the level of the first coordination sphere [30].

The A-site disordered solid solution series $Pr_{1-x}Ba_xMnO_3$ and $Nd_{1-x}Ba_xMnO_3$ exhibit the maximum values of T_C (176 K [31] and 151 K [32]) for $x \sim 0.30$. Disordered $Pr_{0.50}Ba_{0.50}MnO_3$ and $Nd_{0.50}Ba_{0.50}MnO_3$ ($x = 0.50$) have lower T_C values: ∼140 K [33] and ∼80 K [34], respectively. However, the A-site ordered compounds $PrBaMn_2O_6$ and $NdBaMn_2O_6$ (where the A-type antiferromagnetic state is the basic magnetic state [35]) show ferromagnet–paramagnet transitions at ∼320 and ∼310 K [34]. It is interesting to note that such properties are observed only for manganites with the maximal (100%) degree of Ln^{3+} and Ba^{2+} cation ordering. Using special conditions of treatment, a series of solid solutions, $[Ln_gBa_{1-g}]_{Ln}[Ln_{1-g}Ba_g]_{Ba}Mn_2O_6$ with various degrees of A-site ordering from 0 to 100%, has been obtained [36–39]. In this case, the partial A-site disordering suppresses the antiferromagnetism and, as a result, the La^{3+}-, Pr^{3+}- and Nd^{3+}-based solid solutions become pure ferromagnets.

It is important to note that the above examples and discussion refer to solid solutions for which the ratio Ln^{3+}/Ba^{2+} of A-cations is equal to 1/1. Manganites $La_{1-x}Ba_xMnO_3$ with slightly different ratios $x = 0.44$, 0.48, 0.50 and 0.52 have recently been synthesized and studied [40]. All samples in this work [40] have been obtained in the ordered state as single-phase products. It was found that the $x = 0.44$ and 0.48 samples have a purely ferromagnetic ground state, whereas a mixed ferromagnetic/charge-ordered CE-type antiferromagnetic state exists in $x = 0.50$ and 0.52. In addition, the charge-ordered CE-type antiferromagnetic state in $x = 0.52$ was observed to change below $T \sim 180$ K to a more stable orbital-ordered A-type antiferromagnetic state. Yet, the minimal value of the Ba^{2+} cation concentration for which the A-site ordered state can be formed, as well as the synthesis and microscopic details of such a state, have not been determined so far. Here we present the results of our investigation on the structure and magnetotransport properties of A-site disordered and ordered phases in optimally doped $Pr_{0.70}Ba_{0.30}MnO_{3+\delta}$ ($\delta = 0$ and 0.025) manganites with fixed $\langle r_A \rangle = 1.2663$ Å, $\sigma^2 = 0.0178$ Å^2.

2. Experiment

The polycrystalline oxygen stoichiometric A-site disordered $Pr_{0.70}Ba_{0.30}MnO_3$ sample has been obtained using conventional ceramic technology. The oxides Pr_6O_{11} and Mn_2O_3 as well as the carbonate $BaCO_3$ (all of high-purity grade) have been weighed in accordance with the cation ratio Pr/Ba/Mn = 7/3/10 and thoroughly mixed. The resultant mixture was ground in an agate mortar with the addition of a small amount of ethyl alcohol. Since rare-earth oxides are hygroscopic, Pr_6O_{11} was annealed in air for 2 h at $T = 1000\,^{\circ}C$ prior to weighing to remove moisture and carbon dioxide. The obtained chemical mixtures of praseodymium and manganese oxides as well as barium carbonate have been pressed into cylinders 2 cm in diameter and 1.5 cm in height on a hydraulic press in a steel mould under a pressure of about 10^8 Pa. Decarbonization and compaction of the ceramic have been carried out by annealing the sample in air for 2 h at $T = 1100\,^{\circ}C$, followed by crushing. The final synthesis was carried out in air at $T = 1560\,^{\circ}C$ for 2 h. The equation of the chemical reaction for obtaining this initial sample can be written as:

$$(0.70/6)Pr_6O_{11} + 0.30\ BaCO_3 + 0.50\ Mn_2O_3 \rightarrow Pr_{0.70}Ba_{0.30}MnO_3 + 0.30\ CO_2\uparrow. \quad (1)$$

The sample was kept on a platinum substrate during synthesis. Then it was slowly cooled down to room temperature at a rate of 100 °C/1 h to obtain an oxygen content close to the stoichiometric value. Optimally doped manganites, synthesized according to the above-described techniques, are likely to have nearly stoichiometric oxygen concentration [41]. Indeed, the oxygen content, determined by thermogravimetric analysis [42], proved that the parent $Pr_{0.70}Ba_{0.30}MnO_3$ sample synthesized in air for this study was oxygen stoichiometric.

The anion-deficient sample has been obtained by the topotactic reaction. The sample has been placed in an evacuated ($P \sim 10^{-4}$ Pa) and fused quartz ampoule together with a certain amount of metallic tantalum, which has been used as an oxygen getter. The quartz ampoule containing the sample was kept for 24 h at $T = 800$ °C and then cooled to room temperature at a rate of 100 °C/1 h. Reduction was carried out to the phase '$O_{2.60}$' to satisfy the condition $Mn^{3+}/Mn^{2+} = 1$. The equation of this chemical reaction is:

$$Pr_{0.70}Ba_{0.30}MnO_3 + 0.16\ Ta \rightarrow Pr_{0.70}Ba_{0.30}MnO_{2.60} + 0.08\ Ta_2O_5. \quad (2)$$

The oxygen content of the anion-deficient $Pr^{3+}_{0.70}Ba^{2+}_{0.30}Mn^{3+}_{0.50}Mn^{2+}_{0.50}O^{2-}_{2.60}$ sample was determined by weighing before and after the reaction. To reduce the relative error in the measurement of the oxygen content, a sample with a mass of about 3 g was placed in the quartz ampoule. In this case, the relative error did not exceed 0.3%. The anion-deficient sample was then subjected to oxidation in air for 5 h at $T = 800$ °C to obtain the nominal phase 'O_3'. This reaction is described by the following equation:

$$Pr_{0.70}Ba_{0.30}MnO_{2.60} + (0.20 + \delta/2)O_2 \rightarrow Pr_{0.70}Ba_{0.30}MnO_{3+\delta}. \quad (3)$$

After oxidation, the oxygen content was monitored by weighing as well as by chemical titration, and it was determined to be 3.025 ± 0.001. The chemical composition of all the samples was studied by Auger electron spectroscopy (AES) on a PHI Model 660 scanning Auger microprobe. The measurements were performed in high vacuum before and after cleaning the sample's surface with an Ar^+ ion beam. The density of the polycrystalline oxygen stoichiometric A-site disordered $Pr_{0.70}Ba_{0.30}MnO_3$ sample were ~95%, while for the oxygen superstoichiometric A-site ordered $Pr_{0.70}Ba_{0.30}MnO_{3.025}$ sample it is equal ~91%.

X-ray diffraction phase analysis was carried out on a DRON-3M diffractometer using Cu Kα radiation in the angular interval 20 deg $\leqslant 2\Theta \leqslant$ 80 deg. To filter out the Kβ radiation, we used a graphite monochromator. The x-ray diffraction patterns were analysed by the Rietveld method [43] using the software FullProof [44]. Schematic images of the crystal structures were constructed using the program diamond 2.1 [45].

Grain topography imaging was carried out using a Carl Zeiss LEO1455VP scanning electron microscope. The signals from the reflected and secondary electrons were observed simultaneously. Measurements were performed for normal incidence of the beam onto the surface as well as for a tilted sample. X-ray diffraction microscopic analysis was performed using a Röntec energy-dispersive SiLi-semiconductor detector. To ensure a number of pulses at the peaks sufficient for statistical processing, each spectrum was recorded for at least 300 s.

Program-aided calculations of the spectra were performed by comparisons to standard samples, and bremsstrahlung levels provided quantitative analysis results. The distribution of chemical elements in each sample was determined by scanning along a present line. The quantitative stereologic analysis of the electron microscopy images obtained in reflection mode was performed using the 'Autoscan' software (Belarus). The porosity and grain size were obtained from scanning electron microscope images by calibration and fixation of the patterns followed by partitioning and necessary measurement selection. The results are reported as histograms.

Magnetic measurements were carried out on a Quantum Design Physical Property Measurement System (PPMS) in the 3–350 K temperature range for magnetic fields ranging

from −70 to 70 kOe. The temperature dependences of magnetization were measured in a field of 100 Oe in heating mode after zero field cooling (ZFC) and field cooling (FC), as well as in a weak field of 10 Oe immediately after measurements in a relatively strong field of 1 kOe. The field dependences were also measured at temperatures of 3, 20, and 300 K. The Curie temperature T_C was determined from the temperature derivative of the FC curve in a field of 100 Oe as the inflection point ($\min\{dM_{FC}/dT\}$). The spontaneous atomic magnetic moment σ_S was obtained from the field dependence by linear extrapolation to zero field. The dc resistivity of the samples was measured using the standard four-probe technique over a temperature range of 3–350 K. Indium eutectic was employed to deposit the contacts. The magnitoresistance was calculated according to the relation:

$$\mathrm{MR} = \{[\rho(H) - \rho(H = 0)]/\rho(H = 0)\} \times 100\% \tag{4}$$

where MR is the negative isotropic magnetoresistance, $\rho(H)$ is the resistivity in a magnetic field of 50 kOe, and $\rho(H = 0)$ is the resistivity without a magnetic field.

3. Results and discussion

The analysis of the oxygen stoichiometric A-site disordered $Pr_{0.70}Ba_{0.30}MnO_3$ and oxygen superstoichiometric A-site ordered $Pr_{0.70}Ba_{0.30}MnO_{3.025}$ samples by Auger electron spectroscopy (AES) did not reveal any chemical elements other than the main components Pr, Ba, Mn, and O. Figure 1 shows the typical AES spectrum of these samples. Within the experimental accuracy, a 7/3/10 cation ratio was observed for all the samples. The AES measurements were performed in a high vacuum before and after cleaning the sample's surface with a beam of high-energy Ar^+ ions. Consequently, the presence of a carbon (C) peak in the differential spectrum before the high-energy Ar^+ ion treatment can be explained by the adsorption of CO_2 from air onto the manganite surface. This impurity peak disappears upon Ar^+ ion bombardment of the sample's surface.

The analysis of the x-ray diffraction patterns shown in figure 2(a) indicates that the oxygen stoichiometric A-site disordered $Pr_{0.70}Ba_{0.30}MnO_3$ sample is described well ($\chi^2 = 2.77$) by an orthorhombic (SG = $Imma$, $Z = 4$) perovskite-like unit cell (figure 2(a)) with parameters $a = 5.5252(7)$ Å, $b = 7.7672(8)$ Å, $c = 5.5076(7)$ Å and $V = 236.36$ Å^3. These results are in good agreement with previous data [46]. The x-ray diffraction patterns for the oxygen superstoichiometric A-site ordered $Pr_{0.70}Ba_{0.30}MnO_{3.025}$ sample (figure 2(b)) can be calculated satisfactorily ($\chi^2 = 2.91(2.91)$) only if two phases are considered: (i) oxygen stoichiometric A-site ordered $PrBaMn_2O_6$ with a tetragonal (SG = $P4/mmm$, $Z = 2$) unit cell and (ii) oxygen superstoichiometric A-site disordered $Pr_{0.90}Ba_{0.10}MnO_{3.05}$ with an orthorhombic (SG = $Pnma$, $Z = 4$) unit cell. This is also in good agreement with previous data [31]. The volume ratio of the two phases is $V(PrBaMn_2O_6)/V(Ln_{0.90}Ba_{0.10}MnO_{3.05}) \sim 1$. The use of the $Imma$ or $Pnma$ one-phase mode and/or $P4/mmm + Imma$ two-phase mode, as well as the disregard of the tetragonal space group $P4/mmm$, considerably lowers the quality of the Rietveld refinement. The presence of the tetragonal group $P4/mmm$ indicates that the cation ordering is preserved. This type of distortion (SG = $P4/mmm$, $Z = 2$) is associated with ordering of Pr^{3+} and Ba^{2+} cations in the (001) planes, which implies unit cell doubling along the [001] direction. Direct proof of cation ordering is the presence of (0 0 1/2) reflections in the x-ray diffraction patterns, as well as the results of earlier electron diffraction and high-resolution electron microscopy experiments on $PrBaMn_2O_{5.70}$ [34]. The room temperature unit cell parameters, coordinates of ions, average lengths and bond angles, and fit residuals for the perovskite phases of the oxygen stoichiometric A-site disordered $Pr_{0.70}Ba_{0.30}MnO_3$ and oxygen superstoichiometric A-site ordered $Pr_{0.70}Ba_{0.30}MnO_{3.025}$ samples are presented

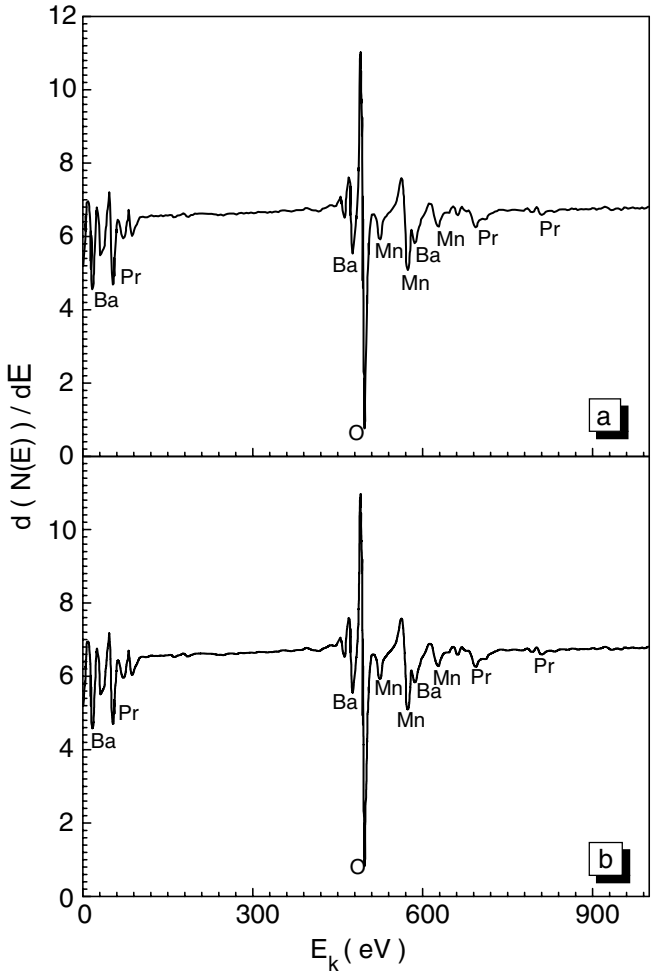

Figure 1. The differential Auger spectrum for the oxygen stoichiometric A-site disordered $Pr_{0.70}Ba_{0.30}MnO_3$ (a) and oxygen superstoichiometric A-site ordered $Pr_{0.70}Ba_{0.30}MnO_{3.025}$ (b) samples after the high-energy Ar^+ ion treatment.

in table 1. Worthy of note is that the ordering of Pr^{3+} and Ba^{2+} cations not only reduces the comparable unit cell volume of the A-site ordered phase by approximately 1% but also increases the average ⟨Mn–O–Mn⟩ bond angle by approximately 6%. It will be shown below that such minute changes in the crystal structure considerably modify the magnetic properties.

Figure 3 shows the crystal structure of the three perovskite phases. The oxygen stoichiometric A-site disordered $Pr_{0.70}Ba_{0.30}MnO_3$ is an aggregate of oxygen octahedrons MnO_6, which are connected at their vertices and spread in all directions (figure 3(a)). The Mn^{3+} and Mn^{4+} ions are located within the oxygen octahedrons MnO_6. The cation distribution is statistical by nature. Most substituted manganites have a distorted unit cell, since the symmetry is lowered compared to its cubic counterpart. There are two types of distortions of an MnO_6 octahedron: (i) due the mismatch between the effective radii of ions and the sizes of the pores occupied by them (size effect) and (ii) due to the Jahn–Teller effect, which is inherent to the Mn^{3+} ion in the high-spin state ($S_{total} = 2$). The oxygen stoichiometric A-site disordered

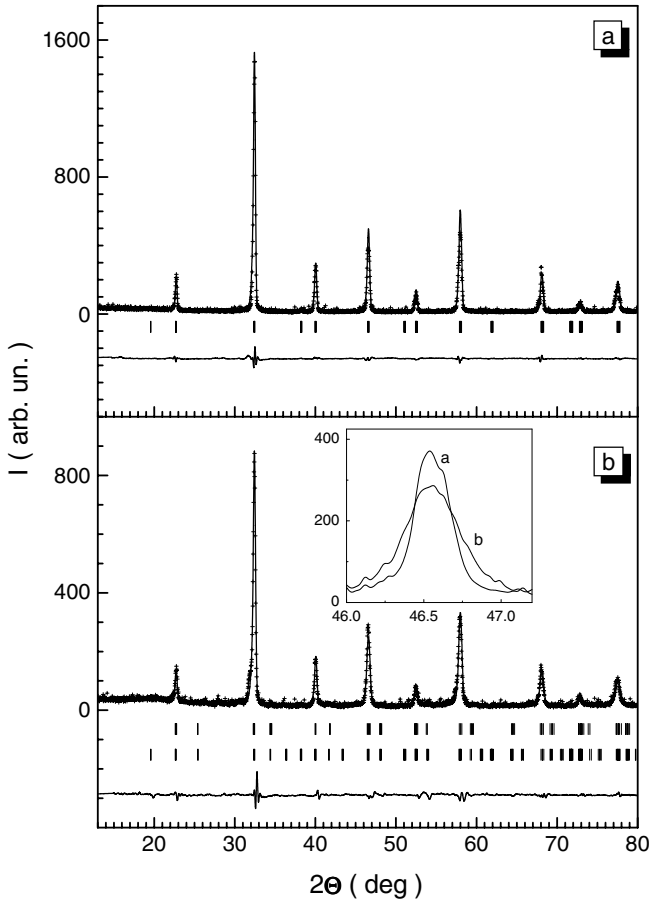

Figure 2. The diagram of powder x-ray diffraction at room temperature for the oxygen stoichiometric A-site disordered $Pr_{0.70}Ba_{0.30}MnO_3$ (a) and oxygen superstoichiometric A-site ordered $Pr_{0.70}Ba_{0.30}MnO_{3.025}$ (b) samples. Experimental data (dark circles), fitting curve (solid curve), admissible positions of Bragg reflections (vertical segment) and the difference curve (lower solid curve). The inset demonstrates the shape and widening of the Bragg reflections.

$Pr_{0.70}Ba_{0.30}MnO_3$ phase has $\langle r_A \rangle = 1.2663$ Å and $\sigma^2 = 0.0178$ Å^2. The free-energy minimum of the crystal structure is attained via the rotation of the MnO_6 octahedron along the unit cell axes and the deformation of the MnO_6 octahedron. A tetragonal distortion takes place if the octahedron rotates about the [100] direction, an orthorhombic distortion is observed in the case of rotation about the [110] axis, and a rhombohedral distortion occurs in the case of rotation about the [111] direction. The two reasons for distortions may be superimposed and may operate simultaneously [47]. For the oxygen stoichiometric A-site disordered $Pr_{0.70}Ba_{0.30}MnO_3$ phase the static cooperative Jahn–Teller effect is removed and distortions occur due to rotation of the MnO_6 octahedron about the [110] direction. The unit cell is orthorhombic (SG = $Imma$, $Z = 4$).

The structure of the oxygen stoichiometric A-site ordered $PrBaMn_2O_6$ phase (figure 3(b-I)) structure is similar to that for the anion-deficient phase [48], with the exception that all the oxygen vacancies are occupied. This phase has $\langle r_A \rangle = 1.3245$ Å and $\sigma^2 = 0.0212$ Å^2. The Mn^{3+}/Mn^{4+} cations are distributed statistically among oxygen octahedrons. For the

Table 1. The structural and refinement parameters for the different phases of the $Pr_{0.70}Ba_{0.30}MnO_{3+\delta}$ samples at room temperature.

Phase	$Pr_{0.70}Ba_{0.30}MnO_3$	$PrBaMn_2O_6$	$Pr_{0.90}Ba_{0.10}MnO_{3.05}$	$Pr_{0.90}Ba_{0.10}MnO_{3.05}$
Space group	*Imma*	*P*4/*mmm*	*Pnma*	*Imma*
a (Å)	5.5252(7)	3.8921(6)	5.5142(6)	5.5222
b (Å)	7.7672(8)	3.8921(6)	7.7806(7)	7.7722
c (Å)	5.5076(7)	7.7625(9)	5.5147(5)	5.5096
V (Å^3)	236.36	117.59	236.60	236.47
$\alpha = \beta = \gamma$ (deg)	90	90	90	90
Pr (*x*, *y*, *z*)	(0, 1/4, −0.004(2))	(0, 0, 0)	(0.021(5), 1/4, 0.999(6))	(0, 1/4, −0.003(4))
Ba (*x*, *y*, *z*)	(0, 1/4, −0.004(2))	(0, 0, 1/2)	(0.021(5), 1/4, 0.999(6))	(0, 1/4, −0.003(4))
Mn (*x*, *y*, *z*)	(0, 0, 1/2)	(1/2, 1/2, 0.249(5))	(0, 0, 1/2)	(0, 0, 1/2)
O1 (*x*, *y*, *z*)	(0, 1/4, 0.435(8))	(1/2, 1/2, 1/2)	(0.469(7), 1/4, 0.012(6))	(0, 1/4, 0.432(3))
O2 (*x*, *y*, *z*)	(3/4, −0.016(5), 1/4)	(1/2, 0, 0.233(7))	(0.219(7), 0.558(6), 0.254(7))	(3/4, −0.014(2), 1/4)
O3 (*x*, *y*, *z*)	—	(1/2, 1/2, 0)	—	—
⟨Mn–O1⟩ (Å)	1.976	1.927	1.956	1.973
⟨Mn–O2⟩ (Å)	1.951	1.945	1.863 and 2.125	1.949
⟨Mn–O3⟩ (Å)	—	1.896	—	—
⟨Mn–O1–Mn⟩ (deg)	158.43	180.00	169.85	157.78
⟨Mn–O2–Mn⟩ (deg)	175.76	175.18	155.32	175.02
⟨Mn–O3–Mn⟩ (deg)	—	180.00	—	—
R_p (%)	9.21	10.42	10.42	12.12
R_{wp} (%)	13.31	14.17	14.17	16.32
R_B (%)	5.32	6.33	6.96	9.56
χ^2 (%)	2.77	2.91	2.91	8.91

oxygen superstoichiometric A-site disordered $Pr_{0.90}Ba_{0.10}MnO_{3.05}$ (figure 3(b-II)), which has $\langle r_A \rangle = 1.2081$ Å and $\sigma^2 = 0.0076$ Å^2, two types of distortion are observed. The Jahn–Teller distortion of the MnO_6 octahedra, in particular, is manifested by a significant increase in the difference between the mean bond lengths ⟨Mn–O1⟩ and ⟨Mn–O2⟩ compared to the initial oxygen stoichiometric A-site disordered $Pr_{0.70}Ba_{0.30}MnO_3$ phase (see table 1). The distortions lead to a change in the space group (SG = *Pnma*, *Z* = 4).

Figure 4 shows the grain topography obtained by scanning electron microscopy for the oxygen stoichiometric A-site disordered $Pr_{0.70}Ba_{0.30}MnO_3$ and oxygen superstoichiometric A-site ordered $Pr_{0.70}Ba_{0.30}MnO_{3.025}$ samples. The noticeable decrease in the average grain size for the oxygen superstoichiometric A-site ordered $Pr_{0.70}Ba_{0.30}MnO_{3.025}$ sample (after the reduction–reoxidization reaction) from micrometre to nanometre size can be explained by the intense diffusion of ions as well as by the ordering of the oxygen vacancies in the shape of complex surfaces over which the destruction of the material occurs. As can be observed, the nanograins combine to form a mosaic structure spanning the entire ceramic. The grain size variation interval for the oxygen superstoichiometric A-site ordered $Pr_{0.70}Ba_{0.30}MnO_{3.025}$ sample is 0.254–0.901 μm, whereas its counterpart for the oxygen stoichiometric A-site disordered $Pr_{0.70}Ba_{0.30}MnO_3$ is 3.817–17.540 μm (table 2). The quantitative stereologic analysis of the oxygen stoichiometric A-site disordered $Pr_{0.70}Ba_{0.30}MnO_3$ sample shows that 19.36% of the grains have a size variation from 10.000 to 12.000 μm. The average grain size is $\langle D \rangle \approx 10.213$ μm. Grains with sizes smaller (0.200 μm) or larger (18.000 μm) have been not

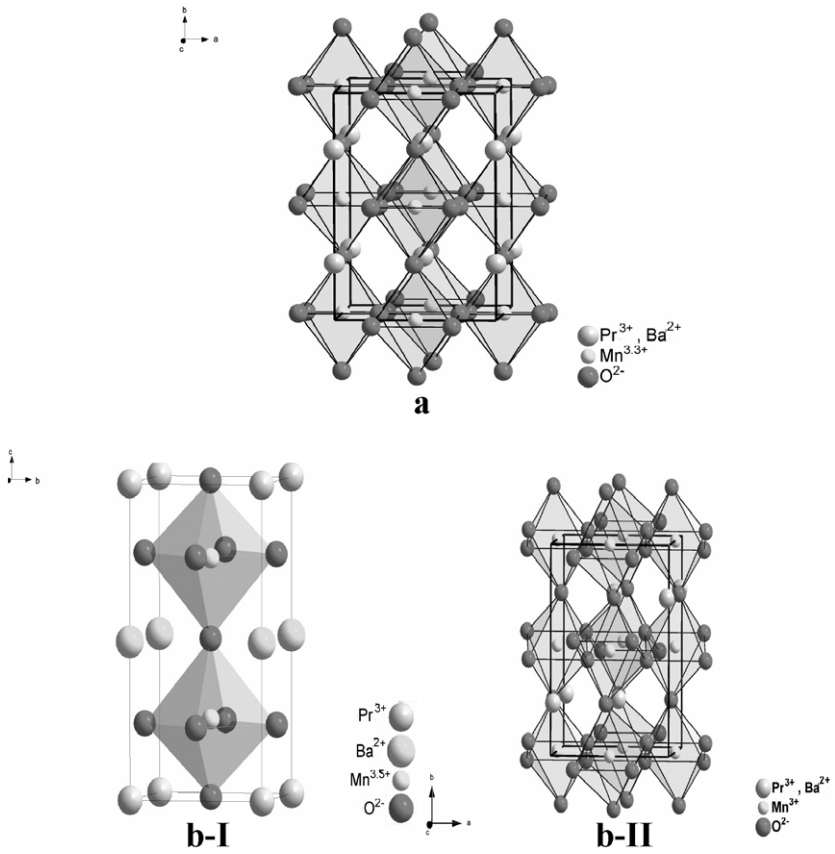

Figure 3. The schematic diagram of the crystal structure for the perovskite phases: the oxygen stoichiometric A-site disordered $Pr_{0.70}Ba_{0.30}MnO_3$ (a), oxygen stoichiometric A-site ordered $PrBaMn_2O_6$ (b-I), and oxygen superstoichiometric A-site disordered $Pr_{0.70}Ba_{0.30}MnO_{3.025}$ (b-II).

detected (figure 5(a)). For the oxygen superstoichiometric A-site ordered $Pr_{0.70}Ba_{0.30}MnO_{3.025}$, 44.30% of the grains have a size variation from 0.400 to 0.600 μm. Grains with a size that is smaller (0.100 μm) or larger (1.000 μm) have been not detected (figure 5(b)). The average grain size for this sample is $\langle D \rangle \approx 0.491$ μm. The shape of the Bragg peaks is affected by the small grain size, which is observed in the inset of figure 2. The A-site ordered $Pr_{0.70}Ba_{0.30}MnO_{3.025}$ sample with nanograins demonstrates the wide Bragg peaks.

The analysis of the chemical phase composition of the oxygen superstoichiometric A-site ordered $Pr_{0.70}Ba_{0.30}MnO_{3.025}$ sample using an energy-dispersion semiconductor detector revealed a nonuniform distribution of the Pr^{3+} and Ba^{2+} cations within nanosized crystallites (figure 4(b)). Regions with cation ratios Pr^{3+}/Ba^{2+} close to 1 and 9 have been observed. This strongly suggests that the ordering of the Pr^{3+} and Ba^{2+} cations in the oxygen superstoichiometric A-site ordered $Pr_{0.70}Ba_{0.30}MnO_{3.025}$ sample occurs via a chemical phase separation on the nanometre scale. The size of the crystallites influences the properties of the crystal structure. A decrease in the grain size (to nanometre size) reduces the unit cell volume, which can be explained by an increase in the surface tension compared to elastic forces in the bulk material [49]. This follows from the comparison of the commensurate unit cell volume of the $Pr_{0.90}Ba_{0.10}MnO_{3.05}$ phase (in our case $V = 236.60$ Å^3) to the previous

Table 2. The results of the quantitative stereologic analysis of the reflection electron microscopy images of the oxygen stoichiometric A-site disordered $Pr_{0.70}Ba_{0.30}MnO_3$ (a) and oxygen superstoichiometric A-site ordered $Pr_{0.70}Ba_{0.30}MnO_{3.025}$ (b) samples.

Sample	a	b
Maximal size (μm)	17.542	0.901
Minimal size (μm)	3.817	0.254
Porosity (%)	3.81	7.96
Simple average (μm)	10.213	0.491
Geometric average (μm)	9.187	0.475
Harmonic average (μm)	8.159	0.461
Sampling variance	2.115	0.018
Sampling mean-square variance	4.599	0.136
Mean-square variance from average	1.387	0.015
Aggregate dispersion	1.923	0.018
Aggregate mean-square variance	4.385	0.135
Relative error	0.0136	0.031
Skewness	0.0133	1.086
Kurtosis	1.735	3.744
Magnitude sum	112.34	38.79
Magnitude quantity	41	79

results ($V = 238.44$ Å^3) [31]. We concluded that the decrease in the unit cell volume in the oxygen superstoichiometric A-site ordered $Pr_{0.70}Ba_{0.30}MnO_{3.025}$ samples occurs as a result of both cation ordering and an increase in surface tension in the outside layers of the nanograins.

The oxygen stoichiometric A-site disordered $Pr_{0.70}Ba_{0.30}MnO_3$ sample is a ferromagnet with a Curie temperature of $T_C \sim 173$ K (figure 6(a)). At the same time, the FC dependence of magnetization for the oxygen superstoichiometric A-site ordered $Pr_{0.70}Ba_{0.30}MnO_{3.025}$ sample exhibits two magnetic transitions at ∼313 and ∼133 K. These correspond to the transition from the ferrimagnetic state to the paramagnetic state for the oxygen stoichiometric A-site ordered $PrBaMn_2O_6$ and oxygen superstoichiometric A-site disordered $Pr_{0.90}Ba_{0.10}MnO_{3.05}$ phases, respectively (figure 6(b)). For this sample, the phase transitions are not particularly sharp, which suggests incomplete ordering of the Pr^{3+} and Ba^{2+} cations in the $PrBaMn_2O_6$ phase. The oxygen superstoichiometric A-site disordered $Pr_{0.90}Ba_{0.10}MnO_{3.05}$ exhibits slightly higher values of $T_C \sim 133$ K compared to the available literature value of $T_C \sim 110$ K [31], which can be attributed to the above-discussed nanocrystallite compression and to the presence of the superstoichiometric Mn^{4+} cations.

The T_C increase for the oxygen superstoichiometric A-site ordered $Pr_{0.70}Ba_{0.30}MnO_{3.025}$ sample is explained by the increase in the average ⟨Mn–O1–Mn⟩ bond angle from 158.43° to 180.00° in the oxygen stoichiometric A-site ordered $PrBaMn_2O_6$ phase (table 1). It is well known that such an increase in the average ⟨Mn–O–Mn⟩ bond angle in manganites leads to an increase in both the e_g-electron bandwidth $W = \cos(1/2[\pi - \langle\text{Mn–O–Mn}\rangle])/\langle\text{Mn–O}\rangle^{3.5}$ and the e_g-electron transfer integral $b_{ij} = b^0_{ij}\cos(\theta_{ij}/2)$ (where $b^0_{ij} \sim \langle\text{Mn–O–Mn}\rangle$ and θ_{ij} is the angle between neighbouring local S_i and S_j spins) [50]. Consequently, the intensity of the indirect superexchange interactions between Mn^{3+}–O–Mn^{3+} increases. Significant variations of the Curie temperature induced by small changes in the average valence bond angle have also been observed by other authors. For example, for optimally doped $Ln_{0.70}D_{0.30}MnO_3$ manganites, an increase in the value of $\cos(1/2)[\pi - \langle\text{Mn–O–Mn}\rangle]$ by just 2% (as a result of the action of the chemical and hydrostatic pressures) almost doubles the value of T_C [20]. For the oxygen superstoichiometric A-site disordered $Pr_{0.90}Ba_{0.10}MnO_{3.05}$ phase we found $T_C \sim 133$ K, which also differs from the literature value of $T_C \sim 110$ K [31].

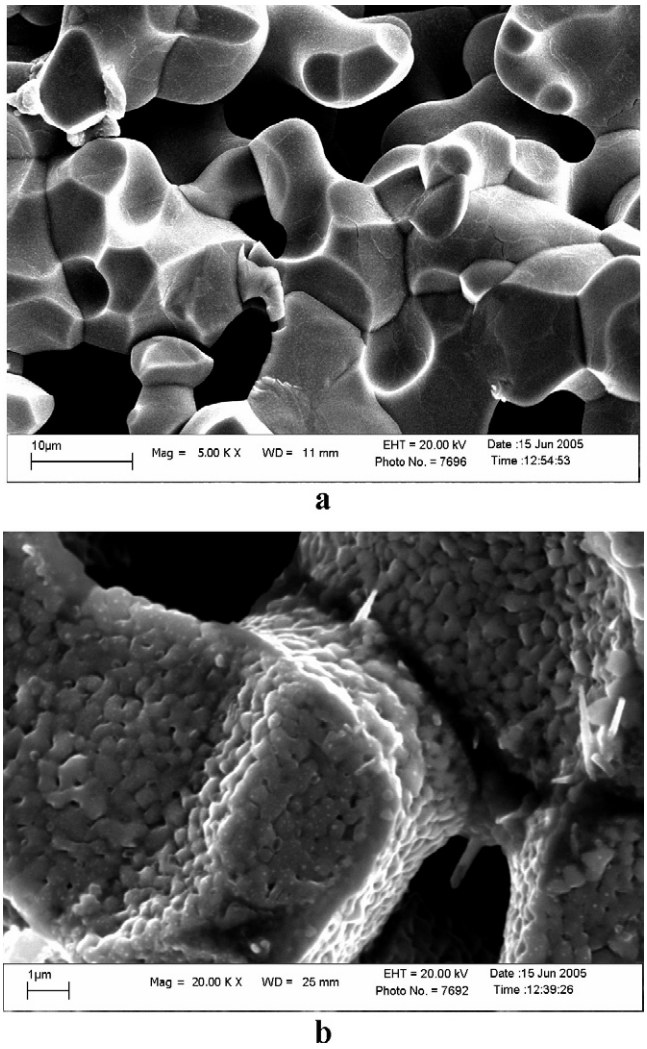

Figure 4. The grain topography obtained with the help of a scanning electron microscope for the oxygen stoichiometric A-site disordered $Pr_{0.70}Ba_{0.30}MnO_3$ (a) and oxygen superstoichiometric A-site ordered $Pr_{0.70}Ba_{0.30}MnO_{3.025}$ (b) samples.

It should be emphasized that the $PrBaMn_2O_6$ and $Pr_{0.90}Ba_{0.10}MnO_{3.05}$ phases are exchanged-coupled. This follows from the results of magnetization measurements in a weak field of 10 Oe (figures 7(I) and (III)) before and after the measurement in a relatively strong field of 1 kOe (figure 7(II)). The magnetization of the oxygen superstoichiometric A-site disordered $Pr_{0.90}Ba_{0.10}MnO_{3.05}$ phase in a field of 10 Oe first increases sharply below ∼136 K (figure 7(I)). A noticeable temperature hysteresis of $\Delta T \sim 22$ K is observed. In the field of 1 kOe, however, an increase in the FC-magnetization curve is observed below $T \sim 126$ K (figure 7(II)) and the hysteresis decreases to $\Delta T \sim 5$ K. After measurements in the strong field of 1 kOe, the magnetization decreases (figure 7(III)) below $T \sim 143$ K. Such a behaviour is preserved for the direct and reverse direction of measurement. This indicates that the high-temperature ferromagnetic phase produces an orienting effect on the low-temperature phase, but an external

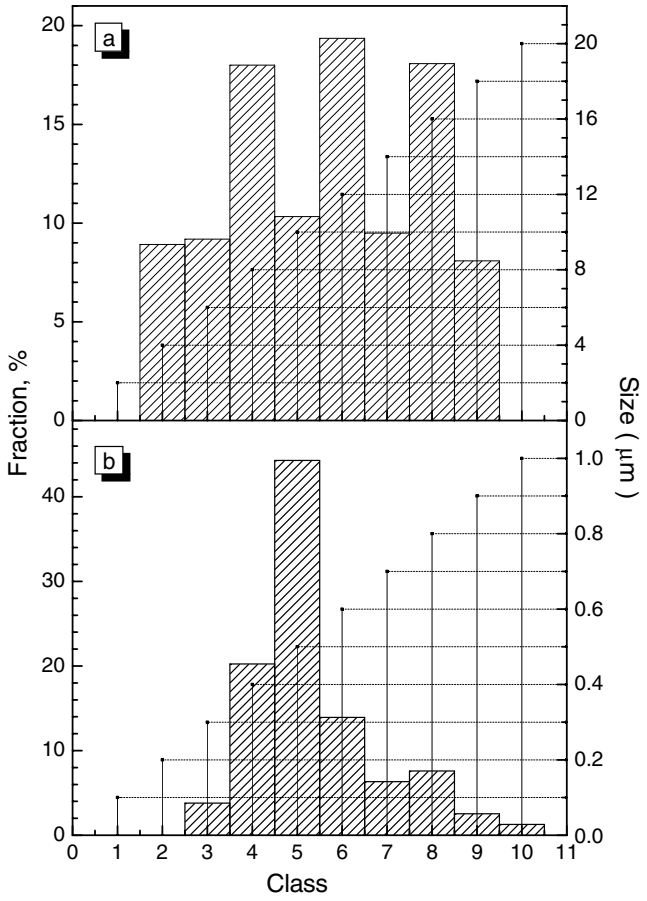

Figure 5. Histogram of the grain size distribution for the oxygen stoichiometric A-site disordered $Pr_{0.70}Ba_{0.30}MnO_3$ (a) and oxygen superstoichiometric A-site ordered $Pr_{0.70}Ba_{0.30}MnO_{3.025}$ (b) samples.

magnetic field suppresses this effect and reduces the sensitivity of the low-temperature phase relative to the high-temperature phase.

Figure 8 shows the field dependence of the atomic magnetic moment for all the samples investigated. The measurements at $T = 20$ K were performed to determine the spontaneous magnetic moment in the ground state and to eliminate the contribution from the Pr^{3+} sublattices. As a rule, the Ln^{3+} sublattice in manganites below $T = 20$ K is oriented antiparallel to the Mn sublattice [51, 52]. In the ground state, the oxygen stoichiometric A-site disordered $Pr_{0.70}Ba_{0.30}MnO_3$ sample has a spontaneous magnetic moment $\sigma_S \sim 3.70$ μ_B/f.u. (Figure 8(I)), whereas for the oxygen superstoichiometric A-site ordered $Pr_{0.70}Ba_{0.30}MnO_{3.025}$ the magnetic moment reaches only $\sigma_S \sim 2.82$ μ_B/f.u. The value $\sigma_S \sim 3.70$ μ_B/f.u. indicates $\sim$100% parallel ordering of all the spins of the $Mn^{3+}(\mu_{total} = 4\ \mu_B)$ and $Mn^{4+}(\mu_{total} = 3\ \mu_B)$ manganese cations. An interesting feature of our results is the substantial difference in the values of spontaneous magnetic moment per formula unit at $T = 20$ K for the oxygen stoichiometric A-site disordered $Pr_{0.70}Ba_{0.30}MnO_3$ ($\sigma_S \sim 3.68$ μ_B/f.u.) and oxygen superstoichiometric A-site ordered $Pr_{0.70}Ba_{0.30}MnO_{3.025}$ ($\sigma_S \sim 2.79$ μ_B/f.u.) (figure 8(II)). In all probability, the nanoceramic contains a considerable fraction of the antiferromagnetic

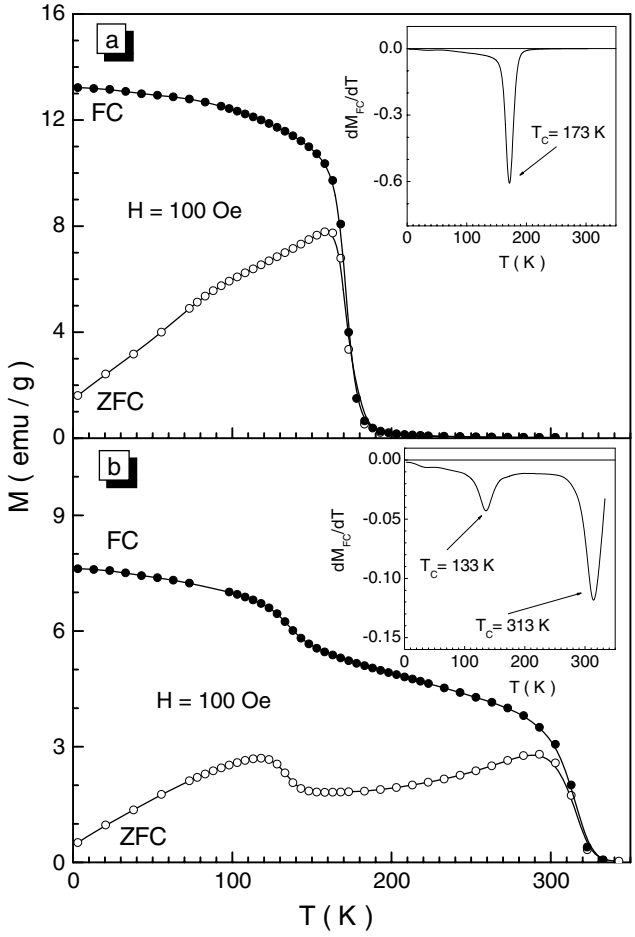

Figure 6. The temperature dependence of the ZFC (open circles) and FC (full circles) specific magnetization in a field of 100 Oe for the oxygen stoichiometric A-site disordered $Pr_{0.70}Ba_{0.30}MnO_3$ (a) and oxygen superstoichiometric A-site ordered $Pr_{0.70}Ba_{0.30}MnO_{3.025}$ (b) samples. The insets show the temperature dependence of the derivative of the FC-magnetization for the corresponding samples.

phase, which, in turn, is a consequence of the exchange bonding frustration in the near-surface layer of the nanograins. At room temperature ($T = 300$ K), the spontaneous magnetic moment per formula unit for the oxygen stoichiometric A-site disordered $Pr_{0.70}Ba_{0.30}MnO_3$ sample is $\sigma_S \sim 0.59\ \mu_B$/f.u. (figure 8(III)). At this temperature, the oxygen superstoichiometric A-site disordered $Pr_{0.90}Ba_{0.10}MnO_{3.05}$ phase is in the paramagnetic state. Taking into account the phase ratio for this sample, we can state that approximately one-fifth of the stoichiometric A-site ordered phase $PrBaMn_2O_6$ at $T = 300$ K is in the ferromagnetic state (for a completely parallel ordering of manganese cations).

Figure 9 illustrates the temperature dependence of the electrical resistivity and magnetoresistance measured in a magnetic field of 50 kOe. The oxygen stoichiometric A-site disordered $Pr_{0.70}Ba_{0.30}MnO_3$ exhibits semiconductor behaviour in the paramagnetic state above ∼173 K (figure 9(a)). This sample has two metal–insulator transitions, at $T_I \sim 128$ and $T_{II} \sim 173$ K. The temperature ∼173 K coincides with the Curie temperature T_C.

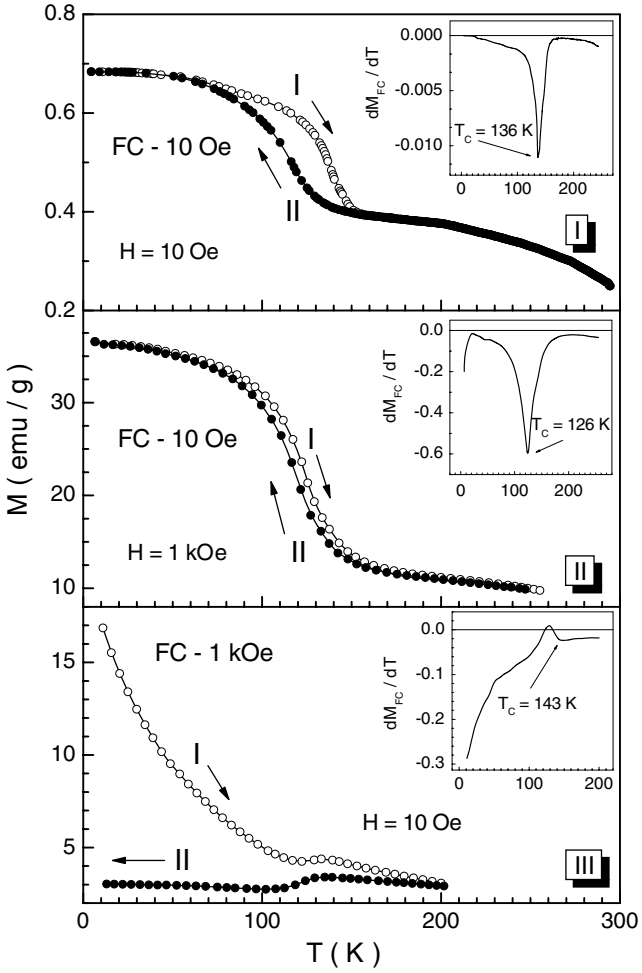

Figure 7. The temperature dependence of the specific FC-magnetization in a field of 10 Oe (I), in a field of 1 kOe (II) and in a field of 10 Oe immediately after the measurement in a field of 1 kOe (III) at the beginning (→) upon an increase in temperature (open circles) and then (←) upon a decrease in temperature (full circles) for the oxygen superstoichiometric A-site ordered $Pr_{0.70}Ba_{0.30}MnO_{3.025}$ sample. The insets show the temperature dependence of the derivative of the FC-magnetization upon an increase in temperature.

Below T_C the ferromagnetic order decreases via magneto-impurity scattering of the charge carriers, and the conductivity shows a metallic behaviour. The metal–insulator transition at $T_I \sim 128$ K for the oxygen stoichiometric A-site disordered $Pr_{0.70}Ba_{0.30}MnO_3$ sample cannot be explained by spin-dependent tunnelling of the charge carriers between grains, because the grains are in the micrometre range and the grain boundaries bring in a small contribution to the resistivity [53, 54]. However, the above-mentioned transition at $T_I \sim 128$ K may be explained by magnetic phase separation in the ferromagnetic and paramagnetic clusters. In [55], the equation for the total resistivity in the ferromagnetic state was obtained as:

$$\frac{\varphi_P(R^{-g} - R_P^{-g})}{R^{-g} + K R_P^{-g}} + \frac{(1-\varphi_P)(R^{-g} - R_F^{-g})}{(R^{-g} + K R_F^{-g})} = 0. \tag{5}$$

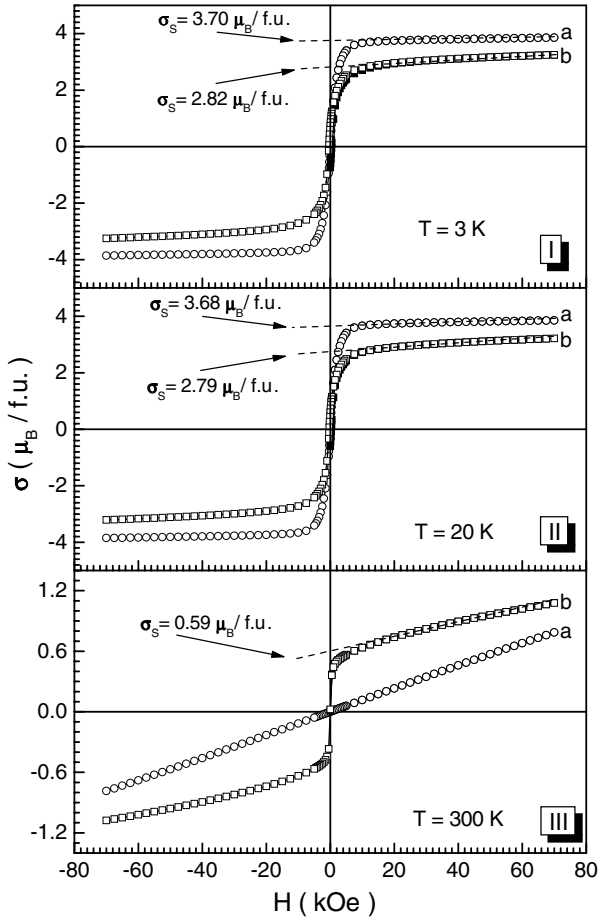

Figure 8. The field dependence of the specific magnetic moment at $T = 3$ K (I), 20 K (II) and 300 K (III) for the oxygen stoichiometric A-site disordered $Pr_{0.70}Ba_{0.30}MnO_3$ (a) and oxygen superstoichiometric A-site ordered $Pr_{0.70}Ba_{0.30}MnO_{3.025}$ (b) samples.

Here, R is the total resistivity, $R_F = B + C(T/T_C)^2$ is the resistivity in the ferromagnetic state (where $(dR_F/dT > 0)$, and B and C are constants), and $R_P = A(T/T_C)\exp(E_{AC}T_C/T)$ is the resistivity in the paramagnetic state (where $(dR_P/dT < 0)$ and A is constant). E_{AC} is the polaron activation energy, and ϕ_P is the volume fraction of the paramegnetic phase (where $\phi_P = 1$ at $T > T_C$ and $\phi_P = \exp[(T/T_C - 1)/d]$, with d the critical parameter of the ferromagnet–paramagnet phase transition and K and g constants that determine the percolation threshold). An electrical resistivity anomaly should be observed at the widening of the ferromagnet–paramagnet transition, below T_C [56]. Also, for $d \geqslant 3.2$ on the resistivity curve, below T_C, the second peak appears. This is observed in our experiments. Switching on the magnetic field reduces the resistivity and increases the metal–insulator transition temperatures to $T_I \sim 138$ K and $T_{II} \sim 210$ K (figure 9(a)). The presence of the magnetic field also induces two peaks in the magnetoresitance: ∼74% and ∼79%. In addition, the A-site ionic ordering leads to an increase in the metal–insulator transition temperature. For the oxygen superstoichiometric A-site ordered $Pr_{0.70}Ba_{0.30}MnO_{3.025}$ sample (figure 9(b)) the transition temperatures are $T_I \sim 128$ and $T_{II} \sim 313$ K. The high-temperature peak almost disappears in a magnetic field, and the

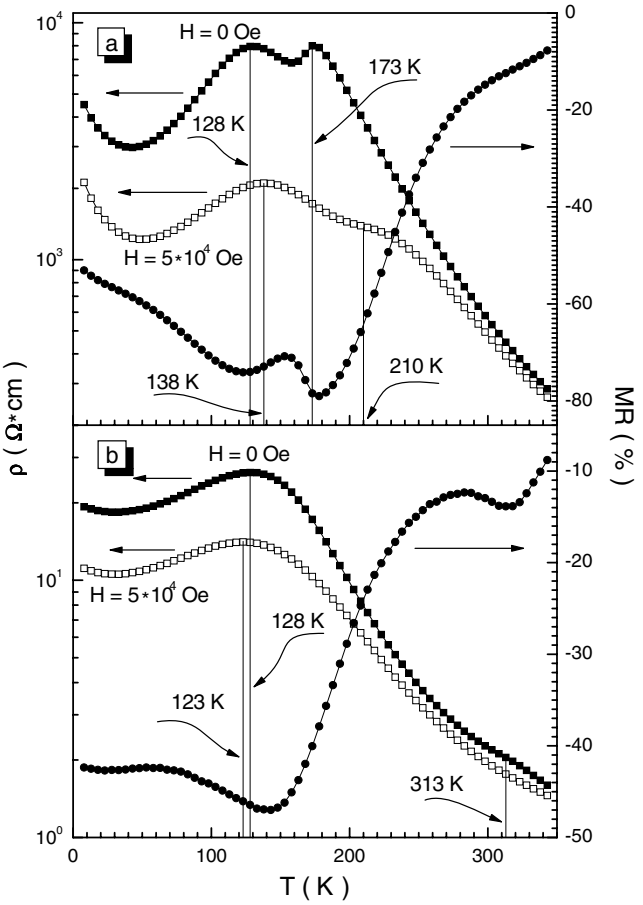

Figure 9. The temperature dependence of the electrical resistivity in the absence of a magnetic field (full rectangles) and in a field of 50 kOe (open rectangles) as well as magnetoresistance (full circles) for the oxygen stoichiometric A-site disordered $Pr_{0.70}Ba_{0.30}MnO_3$ (a) and oxygen superstoichiometric A-site ordered $Pr_{0.70}Ba_{0.30}MnO_{3.025}$ (b) samples.

magnetoresistance at ∼313 K is 14%. The increase in the resistivity transition temperature for the oxygen superstoichiometric A-site ordered $Pr_{0.70}Ba_{0.30}MnO_{3.025}$ sample is probably due to the increase in the e_g-electron bandwidth $W = \cos(1/2[\pi - \langle\text{Mn–O–Mn}\rangle])/\langle\text{Mn–O}\rangle^{3.5}$ and e_g-electron transfer integral $b_{ij} = b^0_{ij}\cos(\theta_{ij}/2)$.

4. Summary

The A-site ordered state has been achieved in samples with $Pr^{3+}/Ba^{2+} \gg 1$ using a 'two-step' reduction–reoxidization method. The parent A-site ionic disordered $Pr_{0.70}Ba_{0.30}MnO_{3+\delta}$ ($\delta = 0$) sample is an orthorhombic (SG $= Imma$, $Z = 4$) ferromagnet with a Curie temperature of $T_C \approx 173$ K, and a ground-state spontaneous magnetic moment of σ_S∼3.70 μ_B/f.u. It also exhibits two metal–insulator transitions at $T_I \sim 128$ and $T_{II} \sim 173$ K, as well as two peaks of magnetoresistance ∼74% and ∼79% in a field of 50 kOe. $Pr_{0.70}Ba_{0.30}MnO_{3+\delta}$ ($\delta = 0$) has grains with an average size of $\langle D\rangle \approx 10.213$ μm. Its successive annealing in vacuum ($P[O_2] \approx 10^{-4}$ Pa) and then in air at $T = 800\,^\circ$C leads to the destruction of the initial grain structure and

to a chemical phase separation into two perovskite phases: (i) oxygen stoichiometric A-site ordered $PrBaMn_2O_6$ with a tetragonal (SG $= P4/mmm$, $Z = 2$) perovskite-like unit cell and a Curie temperature of $T_C \approx 313$ K; and (ii) oxygen superstoichiometric A-site disordered $Pr_{0.90}Ba_{0.10}MnO_{3.05}$ with an orthorhombic (SG $= Pnma$, $Z = 4$) perovskite-like unit cell and a Curie temperature of $T_C \approx 133$ K. The spontaneous magnetic moment for this composite sample in its ground state is $\sigma_S \sim 2.82\ \mu_B$/f.u., whereas, at ∼300 K, $\sigma_S \sim 0.59\ \mu_B$/f.u. The magnetoresistance of the pocessed sample at ∼313 K is ∼14% in a field of 50 kOe. Its average grain size decreases to $\langle D \rangle \approx 491$ nm. The two magnetic phases in the composite sample are exchage coupled. For the $Pr_{0.90}Ba_{0.10}MnO_{3.05}$ phase, the temperature hysteresis is ∼22 K in a field of 10 Oe and ∼5 K in a field of 1 kOe. The magnetic properties of these materials are strongly influenced by the observed chemical phase separation, grain size, and A-site ionic ordering effects.

Acknowledgments

This study has been partly supported by the Belarus Republic Foundation for Basic Research (grant no. F06R-078), a grant from the President of the Republic of Belarus and the Polish State Committee on Research Activities (grant no. 1 P03B 038 27). Work done at The University of Texas at El Paso (UTEP) was supported by the University of Texas Research Fund.

References

[1] Jonker G H and Van Santen J H 1950 *Physica* **16** 337
[2] Van Santen J H and Jonker G H 1950 *Physica* **16** 599
[3] Jonker G H and Van Santen J H 1953 *Physica* **19** 120
[4] Jonker G H 1956 *Physica* **22** 707
[5] Koehler W C and Wollan E O 1957 *J. Phys. Chem. Solids* **2** 100
[6] Von Helmolt R, Wecker J, Holzepfel B, Sehultz L and Samwer K 1993 *Phys. Rev. Lett.* **71** 2331
[7] Chahara K, Ohno T, Kasai M and Kozono Y 1993 *Appl. Phys. Lett.* **63** 1990
[8] Jin S, Tiefel T H, McCormack M, Fastnacht R A, Ramesh R and Chen L H 1994 *Science* **264** 413
[9] Wollan E O and Koehler W C 1955 *Phys. Rev.* **100** 545
[10] Muñoz A, Alonso J A, Martínez-Lope M J and Fernández-Díaz M T 2000 *Solid State Commun.* **113** 227
[11] Hemberger J, Brando M, Wehn R, Ivanov V Yu, Mukhin A A, Balbashov A M and Loidl A 2004 *Phys. Rev.* B **69** 064418
[12] Troyanchuk I O, Khalyavin D D, Trukhanov S V and Szymczak H 1999 *J. Phys.: Condens. Matter* **11** 8707
[13] Sundaresan A, Maignan A and Raveau B 1997 *Phys. Rev.* B **56** 5092
[14] Medarde M, Mesot J, Lacorre P, Rosenkranz S, Fischer P and Gobrecht K 1995 *Phys. Rev.* B **52** 9248
[15] Anderson P W and Hasegawa H 1955 *Phys. Rev.* B **100** 675
[16] Zener C 1951 *Phys. Rev.* **82** 403
[17] De Gennes P-G 1960 *Phys. Rev.* **118** 141
[18] Rodriguez-Martinez L M and Attfield J P 1996 *Phys. Rev.* B **54** 15622
[19] Rodriguez-Martinez L M and Attfield J P 1998 *Phys. Rev.* B **58** 2426
[20] Radaelli P G, Iannone G, Marezio M, Hwang H Y, Cheong S W, Jorgensen J D and Argyriou D N 1997 *Phys. Rev.* B **56** 8265
[21] Vanitha P V, Santhosh P N, Singh R S, Rao C N R and Attfield J P 1999 *Phys. Rev.* B **59** 13539
[22] Goodenough J B 1955 *Phys. Rev.* **100** 564
[23] Goodenough J B, Wold A, Arnott R J and Menyuk N 1961 *Phys. Rev.* **124** 373
[24] Nagaev E L 2001 *Phys. Rep.* **346** 387
[25] Dagotto E, Hotta T and Moreo A 2001 *Phys. Rep.* **344** 1
[26] Millange F, Caignaert V, Domenges B, Raveau B and Suard E 1998 *Chem. Mater.* **10** 1974
[27] Kim B G, Hor Y S and Cheong S W 2001 *Appl. Phys. Lett.* **79** 388
[28] Hwang H Y, Cheong S W, Radaelli P G, Marezio M and Batlogg B 1995 *Phys. Rev. Lett.* **75** 914
[29] Salafranca J and Brey L 2006 *Phys. Rev.* B **73** 214404
[30] Aliaga H, Magnoux D, Moreo A, Poilblanc D, Yunoki S and Dagotto E 2003 *Phys. Rev.* B **68** 104405

[31] Trukhanov S V, Troyanchuk I O, Fita I M, Szymczak H and Bärner K 2001 *J. Magn. Magn. Mater.* **237** 276
[32] Trukhanov S V, Troyanchuk I O, Khalyavin D D, Fita I M, Szymczak H and Bärner K 2002 *JETP* **94** 329
[33] Troyanchuk I O, Trukhanov S V, Szymczak H and Bärner K 2000 *J. Phys.: Condens. Matter* **12** L155
[34] Trukhanov S V, Troyanchuk I O, Hervieu M, Szymczak H and Bärner K 2002 *Phys. Rev.* B **66** 184424
[35] Nakajima T, Kageyama H, Yoshizawa H, Ohoyama K and Ueda Y 2003 *J. Phys. Soc. Japan* **72** 3237
[36] Nakajima T, Yoshizawa H and Ueda Y 2004 *J. Phys. Soc. Japan* **73** 2283
[37] Trukhanov S V 2005 *JETP* **101** 513
[38] Trukhanov S V, Lobanovski L S, Bushinsky M V, Fedotova V V, Troyanchuk I O, Trukhanov A V, Ryzhov V A, Szymczak H, Szymczak R and Baran M 2005 *J. Phys.: Condens. Matter* **17** 6495
[39] Trukhanov S V, Trukhanov A V, Szymczak H, Szymczak R and Baran M 2006 *J. Phys. Chem. Solids* **67** 675
[40] Chmaissem O, Dabrowski B, Kolesnik S, Mais J, Jorgensen J D, Short S, Botez C E and Stephens P W 2005 *Phys. Rev.* B **72** 104426
[41] Schiffer P, Ramirez A P, Bao W and Cheong S W 1995 *Phys. Rev. Lett.* **75** 3336
[42] Trukhanov S V, Lobanovski L S, Bushinsky M V, Khomchenko V A, Pushkarev N V, Troyanchuk I O, Maignan A, Flahaut D, Szymczak H and Szymczak R 2004 *Eur. Phys. J.* B **42** 51
[43] Rodriguez-Carvajal J 1993 *Physica* B **192** 55
[44] http://www-llb.cea.fr/fullweb/winplotr/winplotr.htm
[45] http://www.crystalimpact.com/diamond/v2feature-distang.htm
[46] Boujelben W, Cheikh-Rouhou A, Ellouze M and Joubert J C 2002 *J. Magn. Magn. Mater.* **242–245** 662
[47] Coey J M D, Viret M and von Molnar S 1999 *Adv. Phys.* **48** 167
[48] Caignaert V, Millange F, Domengès B, Raveau B and Suard E 1999 *Chem. Mater.* **11** 930
[49] Shankar K S, Kar S, Subbanna G N and Raychaudhuri A K 2004 *Solid State Commun.* **129** 479
[50] Mahesh R and Itoh M 1999 *Phys. Rev.* B **60** 2994
[51] Fauth F, Suard E, Martin C and Millange F 1998 *Physica* B **241** 427
[52] Toulemonde O, Studer F, Llobet A, Ranno L, Maignan A, Pollert E, Nevriva M, Pellegrin E, Brooks N B and Goedkoop J 1998 *J. Magn. Magn. Mater.* **190** 307
[53] Lee S, Hwang H Y, Shraiman B I, Ratcliff W D and Cheong S W 1999 *Phys. Rev. Lett.* **82** 4508
[54] Ju H L and Sohn H 1997 *Solid State Commun.* **102** 463
[55] McLachlan D S 1987 *J. Phys. C: Solid State Phys.* **20** 865
[56] Tovstolytkin A I, Pogorilyi A N and Kovtun S M 1999 *Low Temp. Phys.* **25** 962